RSC Advances

PAPER

View Article Online
View Journal | View Issue

Check for updates

Cite this: *RSC Adv.*, 2025, **15**, 46048

A study on drug delivery and release kinetics of polyethylene glycol-functionalized few-layer graphene (FLG) incorporated into a gelatin–chitosan bio-composite film

Nahida Sultana,[a] Mehedi Hasan,[a] MD Sami-Ul Alim,[a] Fairuz Tahia,[a] Naoki Komatsu,[b] Khandoker Samaher Salem *[a] and A. F. M. Mustafizur Rahman*[a]

This study develops a composite film by incorporating few-layer graphene (FLG) within a gelatin–chitosan polymer matrix for enhanced drug delivery. The FLG was functionalized in two steps to produce a secondary functionalized FLG (FLG–PEG), resulting in improved dispersion in water, as characterized using an optical microscope. Morphological analysis revealed that FLG–PEG nanosheets are well dispersed, resulting in a smoother, more uniform composite film with the polymer wrapping around them. The functionalized FLG was embedded in a polymeric matrix of chitosan and gelatin, and a bio-composite was prepared by solution casting. FTIR, TGA, and DSC analyses of the samples were conducted to confirm the successful functionalization of the FLG and the increased thermal stability of the composite. Mechanical properties were evaluated, and it was observed that tensile strength and elongation at break increased by 15.41% and 28.90%, respectively, with 0.25% FLG incorporation. Cytotoxicity and antimicrobial assays revealed no adverse cellular effects (95% cell viability) and demonstrated strong antimicrobial activity against both Gram-positive and Gram-negative bacteria, confirming broad-spectrum activity. Uromitexan (Mesna), a cytoprotective adjuvant used during chemotherapy, was incorporated to study its drug-release behavior. The results showed that FLG–PEG composites exhibited rapid and sustained drug release at pH levels of 4.5, 7.0, and 8.0. Mathematical modeling revealed that the drug release kinetics mainly followed the Korsmeyer–Peppas model, driven by both Fickian diffusion (at pH 4.5 and 8.0) and non-Fickian diffusion (at pH 7.0). These findings indicate predictable drug-release behavior of the functionalized composite, suitable for infection-free applications across diverse physiological and pathological environments.

Received 29th July 2025
Accepted 15th November 2025

DOI: 10.1039/d5ra05507e

rsc.li/rsc-advances

Open Access Article. Published on 24 November 2025. Downloaded on 6/7/2026 10:33:14 AM.
This article is licensed under a Creative Commons Attribution-NonCommercial 3.0 Unported Licence.

1. Introduction

Graphene, a single layer of carbon atoms arranged in a two-dimensional hexagonal lattice structure, discovered in 2004, possesses unique properties, such as a large specific surface area (2600 m^2 g^{-1}),[1] high electron mobility (200 000 cm^2 V^{-1} s^{-1}), enhanced electrical (4000 Wm K^{-1}) and thermal conductivity (5000 Wm K^{-1}),[1] extreme optical transparency (97.7%),[2] and exceptional mechanical strength with a high Young's modulus (1000 GPa). The planar structure offers an extraordinary ability to immobilize a wide range of compounds, including drugs, metals, cells, adsorbents, and biomolecules, for diverse applications.[3–6] However, the mass production of single-layer graphene has been significantly hindered for many years due to cost-effectiveness, quality control, and stability. Therefore, few-layer graphene (FLG), composed of a small number of stacked graphene layers, specifically 2–10 layers, has garnered attention because it can be produced at higher yields (about 40%) through more scalable, cost-effective methods.[7] It is also a far superior option to bulk graphite, as bulk graphite possesses poor mechanical, electrical, and thermal properties, and especially low surface area, which is crucial for nanomedicine-based applications. It retains many of graphene's superior attributes, enabling few-layer graphene to serve as an efficient nanocarrier and demonstrating significant potential for the fabrication of effective drug-release systems.[8,9]

Despite its exceptional physicochemical properties, few-layer graphene (FLG) often suffers from limited biocompatibility, cytotoxicity, aggregation, and poor dispersibility when used alone in biological environments, hindering its biomedical and pharmaceutical applications.[10,11] To address this, FLG is functionalized with specific chemical groups that improve its solubility, stability, and biocompatibility in biological fluids.

[a]*Department of Applied Chemistry and Chemical Engineering, University of Dhaka, Dhaka 1000, Bangladesh. E-mail: samaher.salem@du.ac.bd; mustafizacce@du.ac.bd*
[b]*Graduate School of Human and Environmental Studies, Kyoto University, Sakyo-ku, Kyoto 606-8501, Japan*

© 2025 The Author(s). Published by the Royal Society of Chemistry

Open Access Article. Published on 24 November 2025. Downloaded on 6/7/2026 10:33:14 AM. This article is licensed under a Creative Commons Attribution-NonCommercial 3.0 Unported Licence.

Common chemical functionalization involves both non-covalent and covalent bonding. Non-covalent methods primarily rely on π–π interactions, van der Waals forces, or hydrophobic interactions, especially with aromatic molecules, polymers, or biomolecules. In contrast, covalent functionalization attaches molecules or polymers, such as polyethylene glycol (PEG), albumin, poly(lactic acid), poly(lactic-*co*-glycolic) acid, poly(L-histidine), polyaniline, peptides, and ligands, directly to the graphene surface.[3,4,12,13] Among these, surface oxidation of the graphene layer is one of the most convenient functionalization approaches, imparting oxygenated functional groups, including hydroxy (–OH) and carboxy (–COOH) groups, also known as primary functionalization. However, the primary functionalized FLG produces reactive oxygen species (ROS), which reduce its structural and colloidal stability, leading to aggregation in biological fluids. Due to these combined effects, it shows cytotoxicity at higher concentrations, limiting its application in a drug delivery system.[14,15]

The primary functionalization of FLG can be followed by a secondary functionalization, also known as PEGylation, which further significantly increases solubility, biocompatibility, and physiological stability, making it an extremely viable method deployed in the field of drug delivery systems. It provides additional sites for drug attachment and can bind various drugs and their derivatives, thereby increasing bioavailability.[16] PEGylation reduces cytotoxicity and immunogenicity by forming a hydrophilic shield and steric hindrance around FLG.[17,18] It sterically hinders the adsorption of plasma proteins (opsonins) that typically bind to foreign particles and mark them for clearance by organs such as the liver, spleen, and kidneys. Thus, it imparts a stealthy property to FLG–PEG, which evades the immune system, leading to longer circulation times in the bloodstream by reducing recognition or rapid clearance by the immune system.[17] In addition, PEG functional groups can be linked to other molecules (such as folic acid or peptides) to form multi-arm PEGs that facilitate cell-specific drug delivery. The degree of functionalization can be adjusted to control drug loading efficiency and release rate, allowing customization based on therapeutic needs.[18,19]

Polymeric films comprising alginate, PMA (polymethacrylate), chitosan, gelatin, PCL (polycaprolactone), PVA (polyvinyl alcohol), cellulose derivatives, and PLA (polylactic acid) are widely used as carrier matrices in drug delivery systems. In this research, gelatin was selected for its biocompatibility, biodegradability, and favorable film-forming properties. However, the challenge associated with gelatin is its extreme water solubility, limited antimicrobial activity, and low mechanical strength. The limitation is overcome by blending it with chitosan, a cationic polysaccharide that exhibits pronounced exceptional mechanical properties, mucoadhesiveness, film-forming ability, and intrinsic antibacterial activity.[20–25] The gelatin–chitosan composite film is a natural polyelectrolyte, meaning that it carries opposite charges and forms a complex by attracting each other. The positively charged ammonium groups ($-NH_3^+$) in chitosan interact with the negatively charged carboxylate groups ($-COO^-$) in gelatin, resulting in a more physically stable, stronger, and less prone to breaking down film in the presence of water. It binds the drug *via* interactions such as π–π stacking and hydrogen bonding, enabling a consistent, sustained release of the drug over time.[15]

In this paper, we successfully functionalized the FLG with carboxylic acid and polyethylene glycol, and then incorporated it into a gelatin–chitosan matrix. We added Uromitexan (Mesna) drug into the composite and conducted the drug release tests. It is a chemoprotective drug that protects the bladder from the harmful effects of chemotherapy by neutralizing toxic metabolites.[26] The release behavior of the drug from the material under study was assessed under three different buffer conditions: acidic ones at pH 4.5, neutral ones at neutral pH 7.0, and basic ones at pH 8.0. The study demonstrated sustained release for a prolonged duration, providing therapeutic effects by maintaining drug concentrations within the therapeutic window for an extended period. This study demonstrates the successful preparation of biocompatible, strong, and functionally effective gelatin–chitosan–FLG composite films, suitable for effective drug release under various physiological conditions. The presence of FLG not only enhanced the thermal and mechanical properties of the biopolymer matrix but also facilitated sustained drug release, demonstrating good cytocompatibility and antimicrobial activity. These results highlight the potential of FLG-based composites as suitable candidates for future uses in drug delivery systems and biomedical applications.

2. Experimental section

2.1. Materials

Few-layer graphene (FLG) was collected from Japan.[27] Sigma-Aldrich, UK, supplied Gum Arabic (GA). Acetic acid, NaOH, HNO_3, H_2SO_4, DMF, and methanol were sourced from Active Fine Chemicals Ltd, Bangladesh; acetone from Loba Chemie Pvt. Ltd, Mumbai; and PEG from Acme Pharmaceuticals Ltd Thionyl chloride ($SOCl_2$) was purchased from Uni Chem, China, and THF from Daejung Chemicals & Metals Co. Ltd, Korea. CH_3COONa was obtained from Techno Pharmachem, India, and NaH_2PO_4 from Merck KGaA, Germany. Tryptone Soya Agar and Broth were purchased from Oxoid Ltd, UK. Agar powder and potato starch were from Merck Ltd, Mumbai. Glucose was purchased from Nacalai Tesque, Japan. Uromitexan (Mesna) was a product of Baxter Oncology GmbH, Germany. Nylon (Sarlaton) and Teflon filter papers (0.22 μm) were supplied by Square and Incepta Pharmaceuticals Ltd, respectively, in Bangladesh.

2.2. Methodology

2.2.1. Preparation of FLG dispersion. 1g of few-layer graphene (FLG) was dispersed in 100 mL of distilled water containing 1% surfactant (Gum Arabic). The mixture was subjected to ultrasonication for 36 hours in a 200 kHz 50–60 W bath ultrasonicator. Then, the sonicated dispersion was centrifuged at 8000 rpm in a high-speed refrigerated centrifuge for 1 hour, followed by filtration of the solution using a vacuum filter to remove the non-dispersed, agglomerated FLG.[28]

2.2.2. Primary and secondary functionalization of FLG. FLG was functionalized primarily *via* acid oxidation using

Open Access Article. Published on 24 November 2025. Downloaded on 6/7/2026 10:33:14 AM.
This article is licensed under a Creative Commons Attribution-NonCommercial 3.0 Unported Licence.

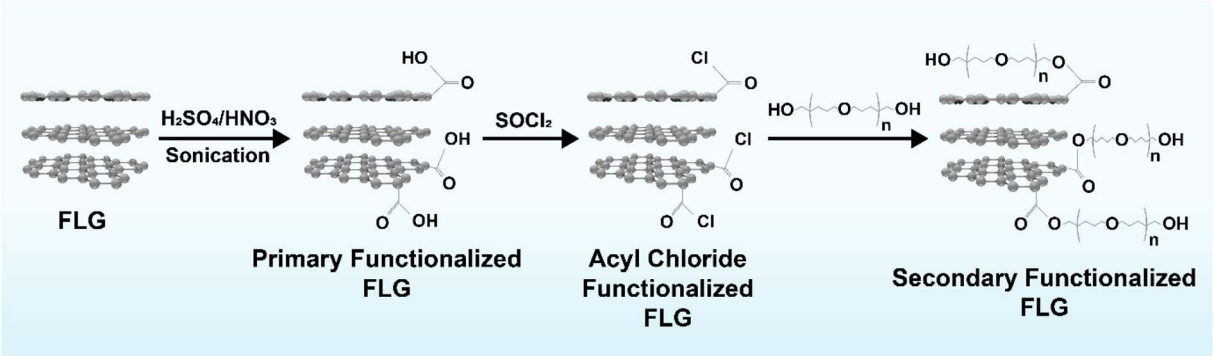

Fig. 1 Reaction scheme of the chemical functionalization of few-layer graphene (FLG). The FLG sheets are first oxidized using a mixture of H_2SO_4 and HNO_3 to introduce carboxy groups (primary functionalization), which are subsequently converted into acyl chlorides using $SOCl_2$. These reactive acyl chloride groups then undergo esterification with polyethylene glycol (PEG) diol, yielding secondary functionalized FLG (FLG–PEG).

a mixture of concentrated sulfuric acid (H_2SO_4, 98%) and nitric acid (HNO_3, 68%) in a 3 : 1 (v/v) ratio. Then, 400 mL of dispersed FLG was added to a 200 mL mixture of acids in a stopper bottle. The treatment was carried out with reflux for 6 hours. After acid treatment, the resultant mixture was filtered using microporous nylon filter paper and then washed with distilled water until the pH value reached 7.0. The neutralized few-layer graphene was then dried at 80 °C for 24 hours to get the dry powder of primary functionalized few-layer graphene (FLG–COOH).[15]

To perform the secondary functionalization of few-layer graphene, 50 mg of primary functionalized FLG was added to 2 mL of anhydrous dimethylformamide (DMF), and ultrasonicated for 5–10 minutes. The dispersion was immediately transferred into 20 mL of thionyl chloride ($SOCl_2$) and then refluxed at 70 °C for 24 hours. After the reaction was completed, the dispersion was thoroughly washed with tetrahydrofuran (THF), filtered, and dried overnight at room temperature. Then, functionalized FLG was added to 5 mL of polyethylene glycol (PEG, 400 g mol^{-1}) and heated to 90 °C. Afterwards, it was stirred for 8 hours. Then, the product was washed with tetrahydrofuran (THF) and filtered through polytetrafluoroethylene (PTFE) filter paper, followed by drying at ambient temperature for 12 hours. The resulting material is referred to as secondary functionalized few-layer graphene (FLG–PEG), as shown in Fig. 1.

2.2.3. Preparation of composites. A 1% (w/v) chitosan solution was prepared by dissolving 1 g of chitosan in 100 mL of 1% acetic acid. Granules of gelatin (10 g) were soaked in 100 mL of distilled water and heated for an hour (35 °C to 37 °C) with

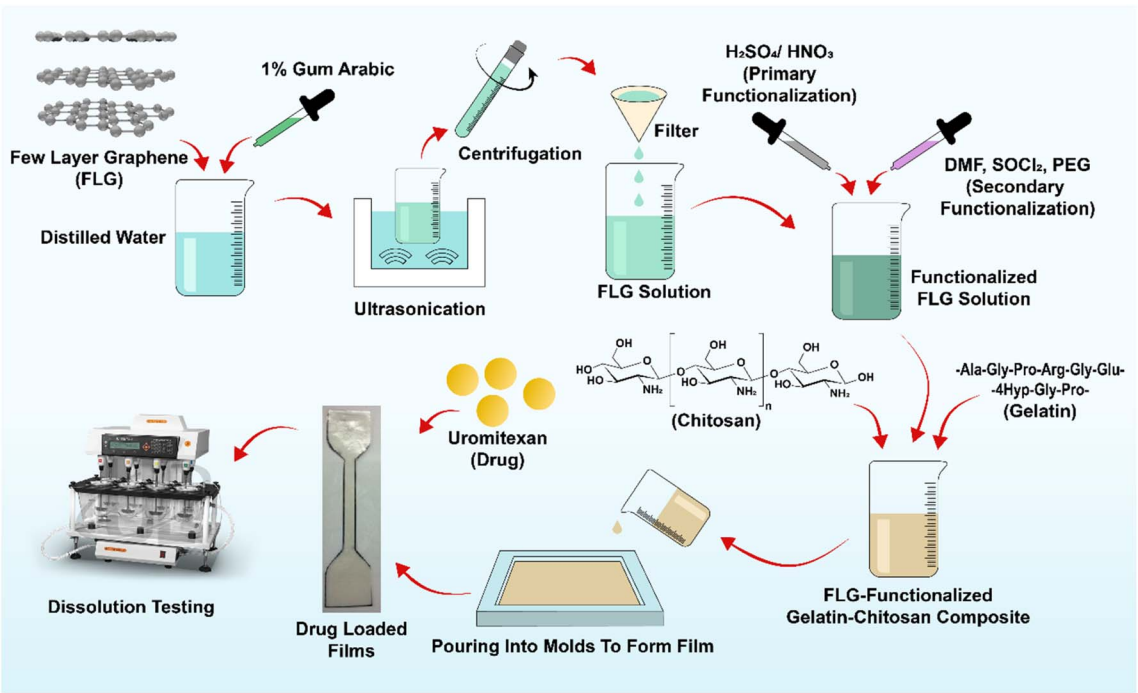

Fig. 2 Schematic workflow showing FLG dispersion and functionalization with COOH and PEG, preparation of gelatin–chitosan polymeric solution, use of solution casting to obtain drug-loaded composite film, and subsequent physicochemical and biological characterization.

© 2025 The Author(s). Published by the Royal Society of Chemistry

Open Access Article. Published on 24 November 2025. Downloaded on 6/7/2026 10:33:14 AM. This article is licensed under a Creative Commons Attribution-NonCommercial 3.0 Unported Licence.

constant stirring. The gelatin–chitosan composite films were prepared by solution casting using different ratios of 10% gelatin and 1% chitosan solution, resulting in dried films containing 0%, 1%, 2%, 3%, 3.5%, 4%, and 4.5% chitosan.[29] FLG was added to 2% gelatin–chitosan solutions at concentrations of 0.1%, 0.25%, 0.50%, 0.75%, and 1% (w/v), stirred for 30 minutes, and sonicated for 1 hour to remove air bubbles. The gelatin–chitosan–FLG mixture was poured into a silicon cloth-covered frame mounted on a flat glass plate for film formulation. The film was dried overnight in a laminar airflow and then peeled off as films (~0.30 mm thick).

2.2.4. Preparation of drug-loaded films. Uromitexan (Mesna) IV solution (400 mg/4 mL vial) was used to prepare drug-loaded films. The drug was added to 0.25% wt/wt gelatin–chitosan–FLG–COOH and gelatin–chitosan–FLG–PEG composite solutions. Then, the drug-containing composite films were prepared using the previously described method (shown in Fig. 2).[20]

2.3. Characterization

The Olympus Culture Microscope, CKX41, equipped with 4×, 10×, 20×, and 40× lenses, was used to capture optical images of the dispersion of FLG in Gum Arabic and a non-surfactant matrix. The ATR and FTIR spectroscopy were performed by an FTIR spectrophotometer, Imprestige-21 model, Shimadzu Corporation (NISHINOKYO-KUWABARACHO, NAKAGYO-KU, KYOTO 604-8511), JAPAN, equipped with an attenuated total reflectance (ATR) device in the wave number range 700–4000 cm^{-1} with a 20-scanning rate with the resolution of 4 cm^{-1}. The FTIR spectra were taken in a transmittance mode. The surface morphology was analyzed using a Zeiss Sigma VP300 FE-SEM (Germany). Before examination, the samples were mounted on conductive carbon tape and then sputter-coated with a thin layer of gold (~5 nm). The tensile strength (TS) and elongation at break (EB%) of the films were determined using a universal testing machine (UTM) from the Hounsfield Series S Testing Machine (UK). The gauge length was set to 110 mm with a constant crosshead speed of 10 mm s^{-1} throughout the experiment. Test specimens were cut into dumbbell or dog-bone shape according to ISO 3167, with a length of 150 mm and a center section measuring 80 mm × 10 mm.[15] The thermogravimetric analysis (TGA) was conducted in a TGA-50H SHIMADZU thermogravimetric analyzer, Japan, from room temperature (25 °C) to 600 °C with a heating rate of 10 °C min^{-1} under a nitrogen atmosphere with a flow rate of 10 mL min^{-1}. The differential scanning calorimetric (DSC) analysis was conducted using a differential scanning calorimeter (Shimadzu, Japan) from room temperature (25 °C) to 600 °C with a heating rate of 10 °C min^{-1} under a nitrogen atmosphere at a flow rate of 20 mL min^{-1}.

2.4. Water and buffer uptake

Water uptake was measured by soaking the films in distilled water contained in a static beaker at 25 °C for up to 96 hours, followed by incubation in phosphate buffer solution (pH 7.0) at 37 °C. After the composite was removed from the solution, it was weighed after being quickly blotted with tissue paper. The swelling behavior of the composite was calculated using the following equation:

$$\text{Water uptake}(\%) = \frac{W_w - W_d}{W_d} \times 100 \quad (1)$$

where W_w is the weight of the wet film and W_d is the weight of the dry film. Results were expressed as a percentage of swelling calculated from eqn (1).

2.5. Cytotoxicity test

The cytotoxic effect of FLG, FLG–COOH, and FLG–PEG was determined by microscopic observation of HeLa cell morphology at the Centre for Advanced Research in Sciences (CARS), University of Dhaka. First, HeLa cells (human cervical carcinoma) were cultured in DMEM (Dulbecco's Modified Eagle's Medium) containing 1% penicillin–streptomycin (1 : 1) and 0.2% gentamycin, as well as 10% fetal bovine serum (FBS). Cells (4×10^4/400 μL) were seeded onto 96-well plates and incubated at 37 °C in a humidified atmosphere containing 5% CO_2 for 24 hours to allow cell attachment. A stock dispersion of 1 g/100 mL was prepared by dispersing FLG, FLG–COOH, and FLG–PEG in sterile distilled water. Working concentrations of 2500, 5000, and 10 000 μg mL^{-1} were obtained by serial dilution. All samples were autoclaved prior to use. Following 24 h pre-incubation, 100 μL of the sample (previously autoclaved) was added to each well. Untreated cells (medium only) served as negative controls. The cytotoxicity was examined under a trinocular inverted light microscope with a camera attachment (Optika, Italy) after 24 hours of incubation. The assay was conducted inside a Biological Safety Cabinet (NU-400E, Nuaire, USA) to ensure aseptic conditions. Each condition was tested in triplicate, and cell viability was expressed as mean ± SD.

2.6. Antimicrobial susceptibility testing

The antibacterial activity of the composite films was evaluated using the standard Kirby–Bauer disk diffusion susceptibility test. A total of four bacterial strains, including selected Gram-positive bacteria (Bacillus subtilis [ATCC 6633] and *Staphylococcus aureus* [ATCC 33591]) and Gram-negative *Escherichia coli* (ATCC 11775) and *Klebsiella pneumoniae* (ATCC 13883), were selected to assess susceptibility patterns. Concisely, Mueller–Hinton Agar (MHA) plates were inoculated with bacterial suspensions adjusted to a 0.5 McFarland standard using sterile cotton swabs. Circular sections of the drug-loaded composite films, cut to the same diameter as standard antibiotic disks (6 mm), were carefully placed on the inoculated Agar medium of the plates. Ciprofloxacin-loaded disks (5 μg) were used as a standard disk to compare the inhibition zones of the drug-loaded composite films. The plates were incubated at 37 °C for 24 h, and the diameters of the inhibition zones (including the disk diameter) were measured with a ruler on the underside of the plate without opening the lid. This was performed in triplicate for each film and bacterial strain, and the average inhibition zone diameter was measured in millimeters.[20,30]

2.7. Drug dissolution test

The dissolution studies were conducted using a Universal Dissolution Tester (UDT-804) from Logan Instruments Corp, USA. Three buffer solutions were used: an acidic buffer (acetate

Open Access Article. Published on 24 November 2025. Downloaded on 6/7/2026 10:33:14 AM. This article is licensed under a Creative Commons Attribution-NonCommercial 3.0 Unported Licence.

buffer, pH 4.5), an alkaline buffer (phosphate buffer, pH 8.0), and a neutral buffer (phosphate buffer, pH 7.0), all at 37 °C. The films (4 cm^2 area, 0.3 mm thickness) were immersed in 900 mL of the respective buffer solution using an overhead stirrer with a blade paddle, and the paddle speed was maintained at 50 rpm. 10 mL of the sample was withdrawn every 10 minutes, and the drug concentration in each sample was estimated using a UV/vis spectrophotometer at its respective wavelength. An equal volume of fresh buffer solution was added after each sample was withdrawn. The amount of Uromitexan (Mesna) released in the buffer solution was determined using a UV-1800 UV/vis spectrophotometer (Shimadzu, Japan) at 204 nm.[31]

2.8. Drug release kinetics

The release kinetics of the gelatin–chitosan–FLG–PEG composite under varying pH were evaluated by fitting the experimental data to four kinetic models as outlined below:

$$\text{(a) Higuchi model: } Q = k_H t^{0.5} \quad \text{(ii)}$$

$$\text{(b) Ritger–Peppas model: } Q = k_R t^{0.6} \quad \text{(iii)}$$

$$\text{(c) Korsmeyer–Peppas model: } Q = k_{KP} t^n \quad \text{(iv)}$$

$$\text{(d) Zero order model: } Q = Q_0 + k_0 t \quad \text{(v)}$$

where Q is the amount of drug released at time t, the drug release constants of Higuchi, Ritger–Peppas, Korsmeyer–Peppas, and zero-order models are denoted by k_H, k_R, k_{KP}, and k_0, respectively. Q_0 is the initial drug amount, and n is the diffusion exponent.[20]

3. Results and discussion

3.1. Structural analysis

Fourier Transform Infrared (FTIR) spectroscopy, as presented in Fig. 3a, was conducted to investigate the functional groups of the functionalized FLG and their gelatin–chitosan composites. The pristine FLG spectrum shows relatively weak peaks due to the lack of surface functional groups. After primary functionalization, the FLG–COOH displays new absorption bands corresponding to the stretching vibrations of –C=O (~1620 cm^{-1}) and –OH groups (broad band around 3400 cm^{-1}), confirming the introduction of a carboxyl group onto the graphene surface.[32] The FLG–PEG spectrum shows a broad peak at approximately 3472 cm^{-1} for the OH band, indicating hydrogen bonding between the PEG and FLG surface groups. In addition, the spectrum of FLG–PEG shows a prominent peak at 2863 cm^{-1} (C–H stretching) and 1110 cm^{-1} (C–O–C stretching). These peaks indicate the successful attachment of polyethylene glycol to the FLG by secondary functionalization.[15]

In Fig. 3b, the FTIR spectra of gelatin–chitosan film show characteristic peaks for both biopolymers, corresponding to broad O–H/N–H stretching bands around 3500–3000 cm^{-1} and amide bands from gelatin around 1650 cm^{-1}, 1550 cm^{-1}, and 1250 cm^{-1}, corresponding to intermolecular interactions such as hydrogen bonding.[15,23] Upon the incorporation of functionalized FLGs, notable changes are observed in the FTIR spectra of the gelatin–chitosan–FLG–COOH and gelatin–chitosan–FLG–PEG composites. Shifts, broadening, and intensity changes in the broad O–H/N–H peak around 3300–3350 cm^{-1} suggest hydrogen bond formation involving the hydroxy and amino groups of the biopolymers. Furthermore, subtle shifts and increased intensity in the Amide I peak around 1650 cm^{-1} and amide II peak at ~1550 cm^{-1} provide evidence of hydrogen bonding between the amide/amino groups of gelatin and chitosan with the carboxy and ether/hydroxy functional groups of the incorporated FLG–COOH or FLG–PEG.[25,33,34] The increase in hydrogen bonding is crucial for achieving homogeneous dispersion of the nanofiller within the polymer matrix and a well-integrated composite network, which directly contributes to the observed improvements in mechanical properties (Fig. 5) and thermal stability (Fig. 6).

3.2. Morphological analysis

The homogeneity of nanoparticle dispersion in the matrix determines the surface area of the nanoparticles available for

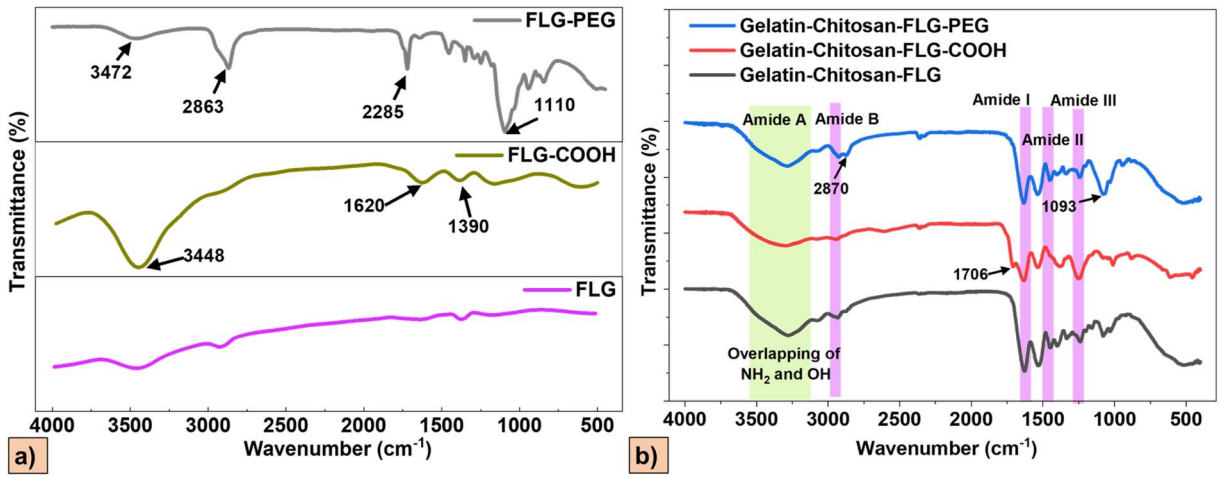

Fig. 3 a) FTIR analysis of FLG, primary functionalized FLG, and secondary functionalized FLG, (b) FTIR analysis of gelatin–chitosan film incorporated with FLG–COOH and FLG–PEG.

© 2025 The Author(s). Published by the Royal Society of Chemistry

Open Access Article. Published on 24 November 2025. Downloaded on 6/7/2026 10:33:14 AM. This article is licensed under a Creative Commons Attribution-NonCommercial 3.0 Unported Licence.

interaction with the matrix and influences different properties of the resulting composites. Optical microscopy images (Fig. 4a and b) reveal a significant difference in the dispersion of FLG in distilled water with and without the use of a surfactant. In the presence of Gum Arabic (Fig. 4a), FLG appears uniformly dispersed, with individual flakes visibly well-separated and evenly distributed throughout the medium. Gum Arabic stabilizes FLG in aqueous solutions by providing steric hindrance and surface charge repulsion that prevent flake restacking.[35] In contrast, in the absence of any surfactant (Fig. 4b), severe agglomeration is evident, indicating poor dispersion stability due to the strong van der Waals forces between graphene layers.

In Fig. 4c, the FE-SEM image of pristine FLG reveals its typical sheet-like morphology, characterised by wrinkled surfaces, stacked layers, and folded edges. Both the surface morphology (Fig. 4d) and cross-sectional view (Fig. 4g) of the pure gelatin–chitosan film appear relatively smooth and homogeneous, without any large aggregates or voids, and exhibit no distinct reinforcement features. However, the FE-SEM images of gelatin–chitosan–FLG–COOH, shown in Fig. 4e (surface view) and Fig. 4h (cross-sectional view), give a rougher surface with particle-like features, showing the aggregation of FLG–COOH nanosheets. This is because the carboxyl groups of the FLG–COOH interact actively with the functional groups of the gelatin–chitosan matrix. This restricts mobility and creates micro-aggregated domains at the surface, resulting in a rougher film morphology. This contrasts with PEG-functionalized FLG, where the flexible PEG chains enhance dispersion and smooth the surface by reducing nanosheet aggregation, as shown in Fig. 4e and i. The PEGylation process masks the sharp edges of the nanosheets and fills interfacial voids, resulting in a more homogeneous interface between the polymer and nanofiller, as evidenced by increased nanosheet thickness due to polymer wrapping. More FE-SEM images of the films at different magnifications are presented in Fig. S1, which are consistent with the above observation.

3.3. Evaluation of mechanical properties

Optimizing chitosan concentration in a composite is essential, as higher concentrations can increase viscosity and introduce structural defects.[24] Therefore, the effect of different concentrations of chitosan and FLG on the mechanical properties of gelatin–chitosan films was evaluated as shown in Fig. 5. Fig. 5a shows that the mechanical properties of the film increased with an initial increase in chitosan concentration, achieving maximum tensile strength at 2% chitosan, after which the properties decreased at higher concentrations. The optimum concentration, which indicates the reinforcing ability of chitosan in biopolymer matrices, is typically associated with increased hydrogen bonding and chain entanglement at moderate

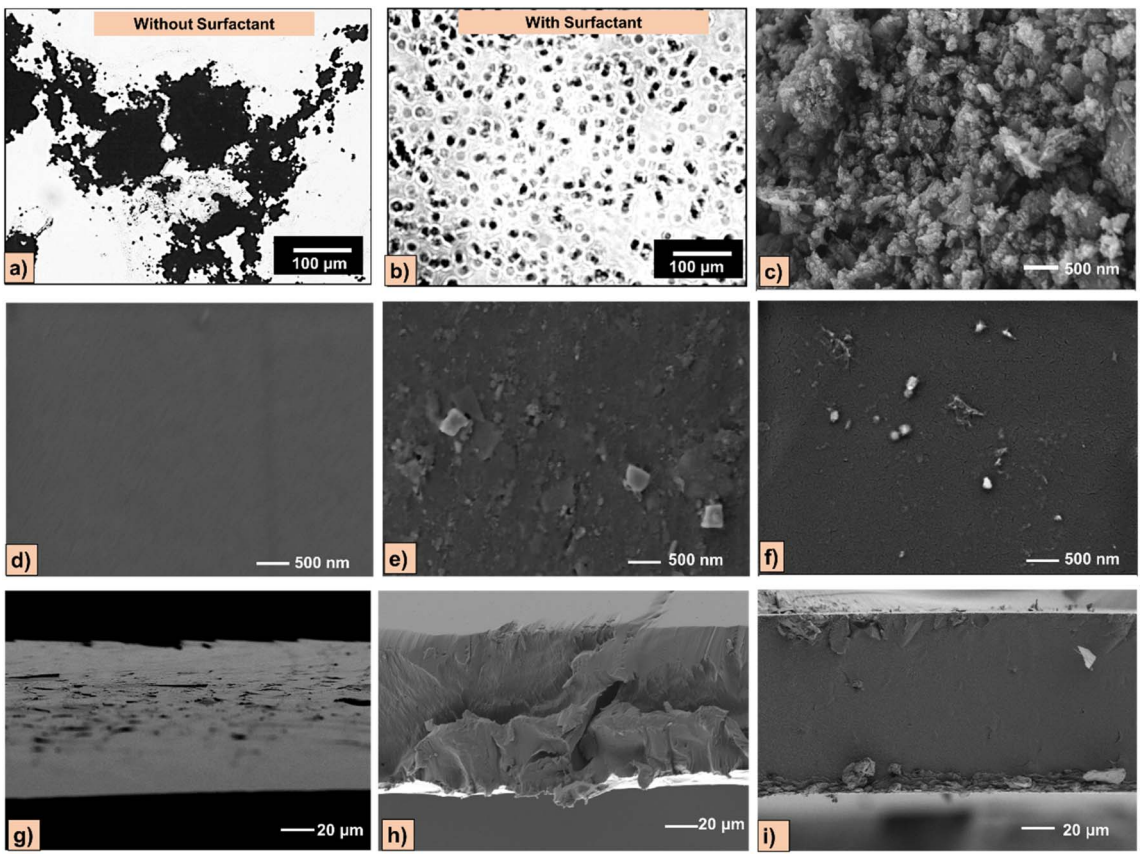

Fig. 4 Optical microscopic images of the FLG dispersed in distilled water, (a) with surfactant and (b) without any surfactant. FE-SEM images of (c) pristine FLG; surface view of (d) gelatin–chitosan film, (e) gelatin–chitosan–FLG–COOH, (f) gelatin–chitosan–FLG–PEG; cross-sectional view of (g) gelatin–chitosan film, (h) gelatin–chitosan–FLG–COOH, (i) gelatin–chitosan–FLG–PEG.

© 2025 The Author(s). Published by the Royal Society of Chemistry

Open Access Article. Published on 24 November 2025. Downloaded on 6/7/2026 10:33:14 AM.
This article is licensed under a Creative Commons Attribution-NonCommercial 3.0 Unported Licence.

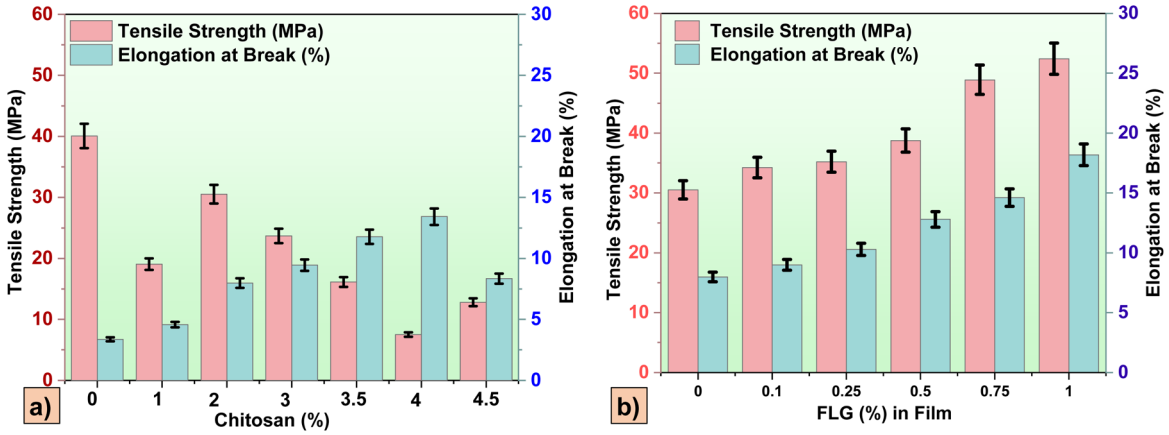

Fig. 5 (a) Mechanical analysis of gelatin–chitosan film at varying chitosan concentration, which shows that at 2% chitosan concentration, the film exhibits the best mechanical capabilities. (b) Mechanical analysis of the composite at varying FLG concentration, which illustrates enhanced mechanical properties following FLG incorporation.

concentrations.[36] However, high amounts can diminish this effect, causing aggregation or phase separation and thus reducing mechanical integrity.[37] Concurrently, elongation at break generally increased with chitosan concentration, indicating enhanced flexibility, a common characteristic when polysaccharides like chitosan are incorporated into protein-based films.[38] Furthermore, Fig. 5b distinctly illustrates the significant improvement in the mechanical performance of the composite films with the incorporation of FLG. Both tensile strength and elongation at break exhibited a consistent and substantial increase with rising FLG concentration, reaching their highest values at a 1% FLG concentration. This profound reinforcement is attributed to the high aspect ratio, large surface area, and high Young's modulus of FLG, which enable effective stress transfer within the polymer matrix, prevent crack propagation, and simultaneously enhance both strength and ductility.[39] Besides, strong interfacial interactions due to covalent bonding through functional groups and π–π stacking, FLG anchors the polymer chains of gelatin–chitosan film to its surface. Hence, upon tensile loading, stress is transferred across the FLG–polymer interface, thereby distributing the load and increasing the composite's ultimate strength and elongation at break.[6] However, even though the mechanical property improved with an increase in FLG concentration, the ideal loading concentration of FLG in the polymeric film was taken as 0.25 wt%, considering the reduced biocompatibility of FLG due to an increase in cytotoxic effect at the elevated concentrations, shown in Fig. 8.

3.4. Thermal performance analysis

The thermal performance of the prepared films was analyzed *via* thermogravimetric analysis (TGA), as presented in Fig. 6a. All samples undergo an initial 8–10% weight loss between 110 and 210 °C due to the evaporation of absorbed moisture and the release of small amounts of NH_3 and CO_2, a common phenomenon in biopolymer films.[40] Following this, pure gelatin and pure chitosan exhibit major degradation steps (~57% weight loss) at approximately 220–330 °C, reflecting the decomposition of their respective polymer backbones. The final degradation starts at 350 °C due to the breakdown of gelatin's intermolecular hydrogen bonds and partial cleavage of its polypeptide chains,

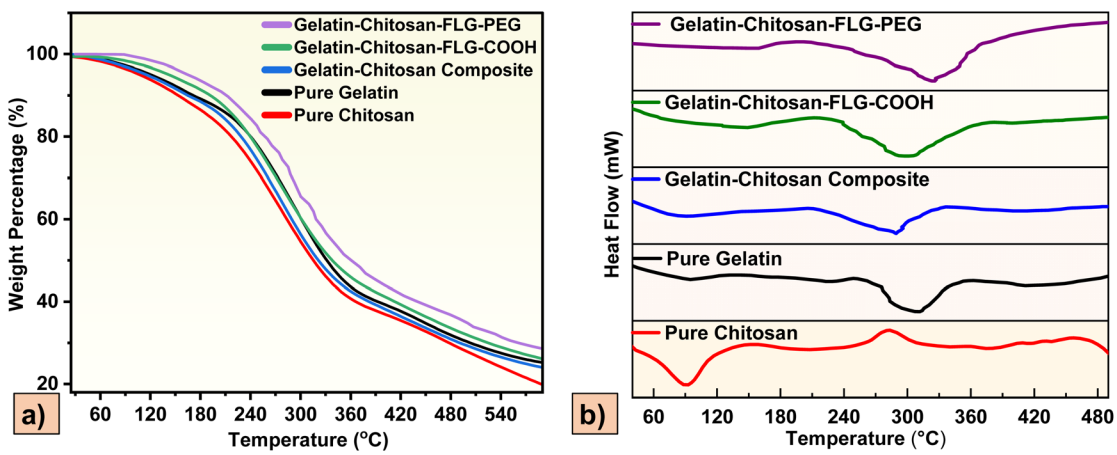

Fig. 6 (a) Thermogravimetric analysis (TGA) curves, and (b) differential scanning calorimetry (DSC) thermograms of the prepared bio-composite films, highlighting improved thermal properties due to functionalization.

© 2025 The Author(s). Published by the Royal Society of Chemistry

Open Access Article. Published on 24 November 2025. Downloaded on 6/7/2026 10:33:14 AM. This article is licensed under a Creative Commons Attribution-NonCommercial 3.0 Unported Licence.

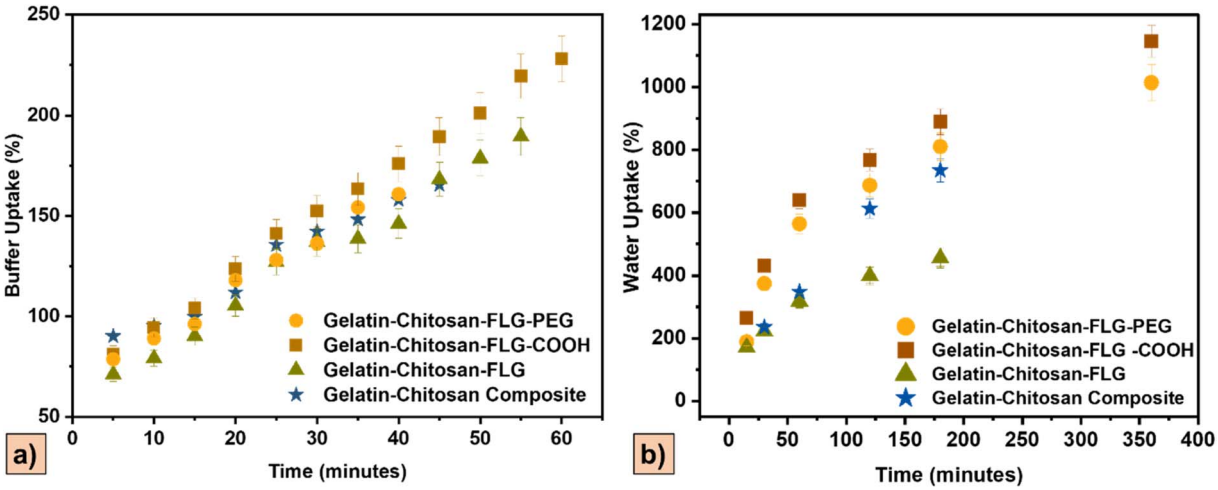

Fig. 7 The image showing scatter plots of (a) buffer uptake (%) of gelatin–chitosan-based composites as a function of time (0–60 minutes), showing enhanced buffer absorption in functionalized FLG composites, particularly gelatin–chitosan–FLG–COOH. (b) Water uptake (%) over time (0–360 minutes), showing sustained swelling behavior, showing the highest uptake in gelatin–chitosan–FLG–COOH composite, indicating improved hydrophilicity due to increased surface functional groups.

leading to a significant weight loss, followed by final combustion beginning at 450 °C, leading to more than 90% weight loss.[15] However, gelatin–chitosan–FLG–COOH and gelatin–chitosan–FLG–PEG composites demonstrate a notable shift in their degradation curves towards higher temperatures, attributed to the successful functionalization of FLG. This improved thermal stability is attributed to graphene-based nanofillers acting as effective heat barriers, radical scavengers, and mass-transport inhibitors within the polymer matrix, thereby delaying thermal decomposition and increasing char yield.[41,42]

Concurrently, the thermal behavior of the composite film was evaluated using differential scanning calorimetry (DSC), as shown in Fig. 6b. The DSC thermograms corroborate the TGA findings, showing a shift in the thermal transitions of the polymer matrix upon incorporation of FLG. For chitosan, endothermic and exothermic peaks are observed at approximately 100 °C and 270 °C, respectively. This endothermic peak corresponds to the energy required to remove the bound and adsorbed water on the hydrophilic surface of chitosan. The exothermic peak indicates the thermal degradation and decomposition of the chitosan, which involves the breakdown of amine and *N*-acetyl groups and the release of volatile products.[43] Additionally, in the DSC thermograms of gelatin and all composite films, an endothermic peak is observed around 300–350 °C, indicating the thermal degradation of the gelatin structure due to the breaking of intermolecular bonds. It moves to higher temperatures for films embedded with primary and secondary functionalized groups. The delayed degradation exotherm indicates a higher activation energy barrier for the thermal scission of the polymer backbone, suggesting a thermally resilient polymer-filler interphase. In addition, due to the incorporation of functionalized FLG, the glass transition temperature shifts to a higher value, requiring more heat to break the intermolecular bonding in the composite films, resulting from the restricted segmental movement of the associated polymer chains within the composite films.[44]

From both TGA and DSC, it is observed that FLG–PEG provides superior reinforcement compared to FLG–COOH, thereby improving the thermal properties of gelatin–chitosan films, as confirmed by a higher T_g (glass transition temperature), T_m (melting temperature), a higher decomposition onset, a delayed thermal transition, and slower breakdown data. This is due to the better hydrogen bonding and crosslinking properties of PEG, which form an effective network in the composite film. Besides, FLG–COOH tends to aggregate and cause defects in the biopolymer matrix, which can be avoided by the secondary functionalization using PEG.

3.5. Swelling behavior

To evaluate the effect of functionalization on the swelling behavior of the polymeric composite films, the prepared samples were assessed through time-dependent buffer uptake (Fig. 7a) and water uptake (Fig. 7b). All composite films demonstrated the ability to absorb water and buffer, but a notable shift in uptake properties was observed due to the change in functional groups. For example, the gelatin–chitosan–FLG composite exhibited reduced water and buffer uptake compared to the gelatin–chitosan composite, owing to the incorporation of a hydrophobic graphene layer into the film, which hindered solvent penetration and diffusion. Furthermore, a significant increase in water and buffer uptake was observed in the gelatin–chitosan–FLG–COOH composite due to the incorporation of highly polar carboxy (–COOH) groups on the graphene surface. It significantly increases the material's affinity for water through hydrogen bonding and electrostatic interactions, thereby facilitating greater solvent diffusion and absorption. This sustained and swelling capacity highlights the effectiveness of functionalization in performing drug release in different physiological conditions.[34,45]

Gelatin–chitosan–FLG–PEG showed significantly higher uptake in water and buffer than all other composite films,

Open Access Article. Published on 24 November 2025. Downloaded on 6/7/2026 10:33:14 AM. This article is licensed under a Creative Commons Attribution-NonCommercial 3.0 Unported Licence.

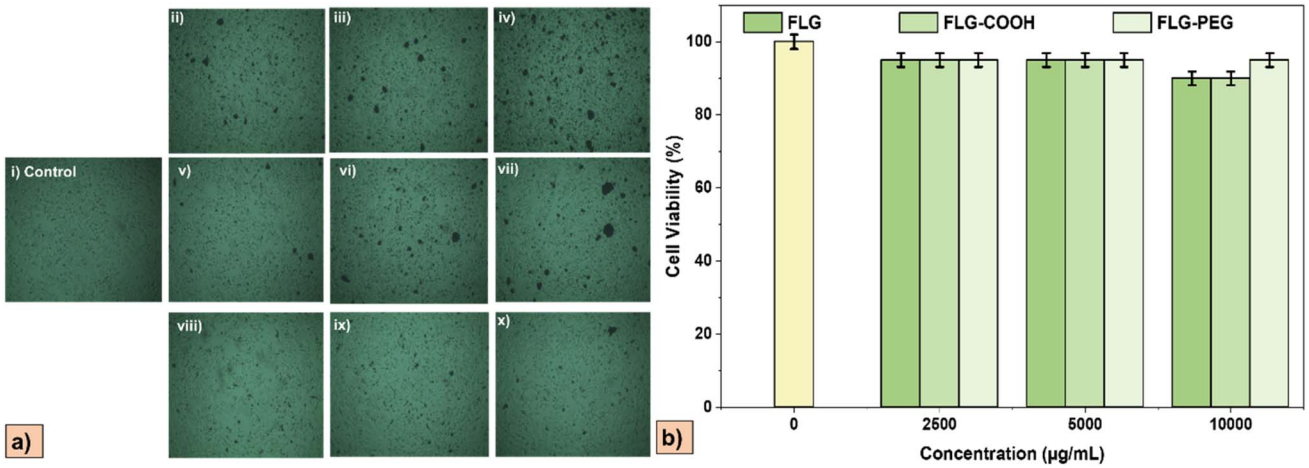

Fig. 8 (a) Microscopic images of HeLa cells treated with FLG aqueous dispersions at varying concentrations: (i) control, (ii) 2500 μg mL^{-1}, (iii) 5000 μg mL^{-1} and (iv) 10 000 μg mL^{-1} of pristine FLG; (v) 2500 μg mL^{-1}, (vi) 5000 μg mL^{-1}, and (vii) 10 000 μg mL^{-1} of primarily functionalized FLG; (vii) 2500 μg mL^{-1}, (ix) 5000 μg mL^{-1}, and (x) 10 000 μg mL^{-1} of secondarily functionalized FLG. (b) A bar chart showing cell viability (%) of HeLa cells after 24 hours of exposure to control and different concentrations (2500, 5000, and 10 000 μg mL^{-1}) of FLG, FLG–COOH, and FLG–PEG dispersions.

except gelatin–chitosan–FLG–COOH. This is due to the cross-linking ability of PEG, which hinders solvent penetration in water and buffer media.[18] However, the reduced water and buffer uptake observed in the PEG-functionalized composite prevents overly rapid swelling and disruption of the polymer matrix. Therefore, compared to the carboxy-functionalized composite, the PEG-functionalized system offers additional benefits without significantly compromising the desirable uptake characteristics of the carboxy-functionalized film.

3.6. Cytotoxic analysis

To assess the change in biocompatibility following the functionalization, cytotoxicity analyses were conducted *in vitro* using HeLa cells for FLG, FLG–COOH, and FLG–PEG, and the results are shown in Fig. 8. Microscopic images in Fig. 8a display a dose-dependent cytotoxicity, which is quantified in Fig. 8b by a bar chart showing the relationship between cell viability and the different concentrations of the respective samples. The data indicate a slight decrease in biocompatibility at elevated FLG concentrations, as confirmed by 90% cell viability at 10 000 μg mL^{-1}, compared to 95% at 5000 μg mL^{-1}. The primary functionalization composite also showed slight cytotoxicity, showing 95% cell viability at 10 000 μg mL^{-1}. Notably, FLG–PEG outperformed all other samples, maintaining a consistent 95% cell viability across all testing concentrations, thereby proving the effectiveness of the secondary functionalization in imparting biocompatibility to the drug carrier composite.

The cytotoxicity of FLG at higher concentrations is attributed to its hydrophobic surface, and that of FLG–COOH at elevated concentrations is due to the generation of reactive oxygen species (ROS).[46,47] The FLG interacts with the phospholipid bilayer of the cell membrane, leading to cytoskeletal disruption. Furthermore, the sharpened edges of FLG can be inserted and cut through the cell membrane, thereby destroying it.[14] FLG–COOH increases intracellular ROS levels, leading to oxidative stress and potential cell damage, as shown by Lammel *et al.*[48,49] Functionalization with PEG groups improves biocompatibility

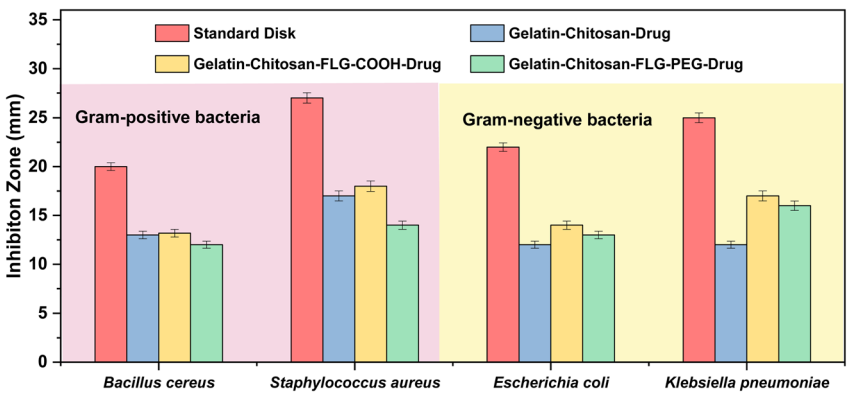

Fig. 9 Antibacterial activity was measured by the diameter of the inhibition zone (mm) of composites, including gelatin–chitosan-drug, gelatin–chitosan–FLG–COOH–drug, gelatin–chitosan–FLG–PEG-drug, and a standard antibiotic disk as a control against common pathogenic bacteria, such as Gram-positive (*Bacillus cereus*, *Staphylococcus aureus*), and Gram-negative (*Escherichia coli*, and *Klebsiella pneumoniae*).

© 2025 The Author(s). Published by the Royal Society of Chemistry

Open Access Article. Published on 24 November 2025. Downloaded on 6/7/2026 10:33:14 AM. This article is licensed under a Creative Commons Attribution-NonCommercial 3.0 Unported Licence.

by reducing hydrophobic interactions and ROS generation, thereby minimizing harmful interactions with cells. PEGylation, in particular, outperforms carboxylation due to its ability to evade detection and immune recognition through hydrophilic shielding, and its crosslinking ability can mask sharp edges, making it the most biocompatible for drug delivery.[16–18]

3.7. Evaluation of antimicrobial susceptibility

Antibacterial activity of the composite films was assessed using the disk diffusion method against Gram-negative and Gram-positive bacterial strains to evaluate the composites' broad-spectrum effectiveness, as shown in Fig. 9. The optical images of the inhibition zone, along with the respective disks of the method, are presented in Fig. S2–S5. The gelatin–chitosan-drug composite exhibited inherent antibacterial activity, a characteristic of chitosan's polycationic nature, which interacts with the negatively charged bacterial cell membranes, leading to membrane disruption and leakage of intracellular contents.[50] However, a significant enhancement in antibacterial activity was observed upon the incorporation of functionalized FLG. Specifically, the gelatin–chitosanFLG–COOH–drug composite exhibited superior antibacterial activity across all tested bacterial strains compared to the non-functionalized gelatin–chitosan-drug composite. This is attributed to the intrinsic antibacterial properties of FLG–COOH, which produces reactive oxygen species (ROS) that induce oxidative stress in bacterial cells and damage their membranes.[51,52] Under incubation conditions, FLG–COOH promotes light-independent electron transfer from biological components to dissolved O_2 in the medium. Here, carboxyl groups and defect sites on FLG act as electron-accepting centers and transfer electrons to O_2, producing $O_2^{\bullet-}$, H_2O_2, $^{\bullet}OH$ that damage the membrane lipids, proteins, and DNA.[53]

The gelatin–chitosan–FLG–PEG-drug exhibited slightly lower antimicrobial activity compared to gelatin–chitosan–FLG–COOH–drug. This is due to the PEG hydration layer, which blocks direct contact between the bacterial membranes.[17,19] However, the antimicrobial response of gelatin–chitosan–FLG–PEG-drug is well above the required level for application in drug delivery systems. Furthermore, it exhibited strong antibacterial activity against both Gram-positive and Gram-negative bacteria, suggesting potential for broad-spectrum antimicrobial activity.

3.8. Drug release profile

The release profile of the drug from gelatin–chitosan composite, gelatin–chitosan–FLG–COOH, and gelatin–chitosan–FLG–PEG was evaluated at pH 4.5, 7.0, and 8.0, as presented in Fig. 10a–c, respectively. Both the FLG–COOH and the FLG–PEG exhibited a near-complete release (as high as 100%) within 70–90 minutes across a range of pH environments, mimicking real physiological conditions. This is attributed to the presence of functionalized few-layer graphene (FLG) within the polymer matrix that enhances buffer uptake, improves solvent penetration, and creates more porous structures. The drug release at pH 4.5 (Fig. 10a) suggests that the acidic environment enhances diffusion and drug dissolution from the functionalized composites, making it suitable for targeted drug delivery in the fed stomach,

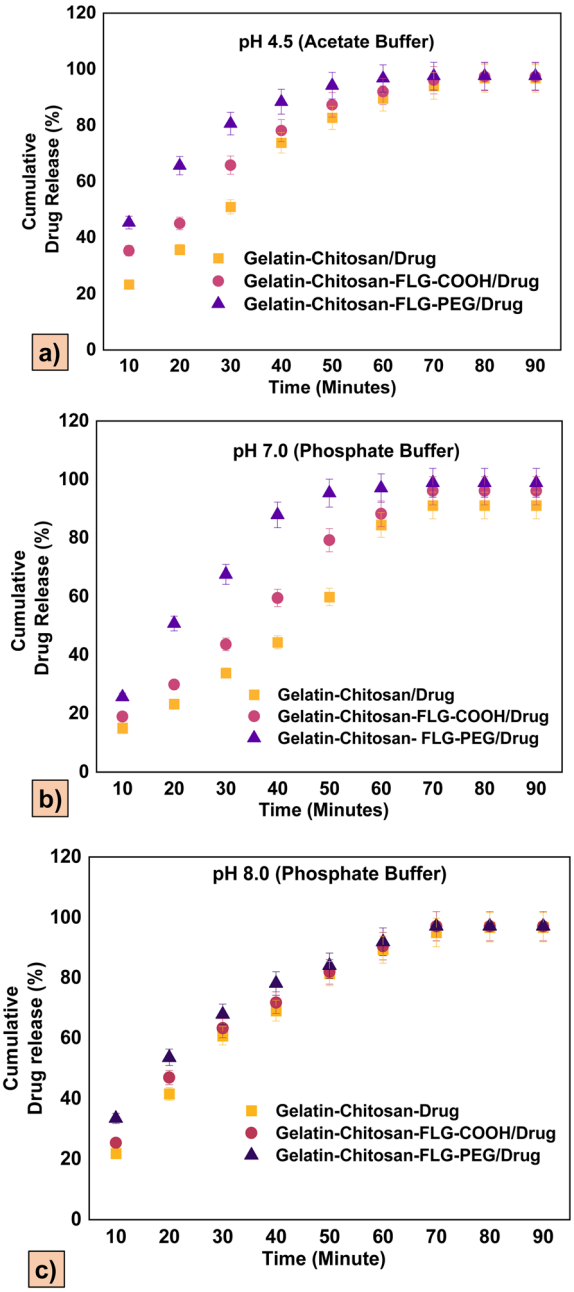

Fig. 10 Scattered plots showing drug release profiles of plain gelatin–chitosan composite, gelatin–chitosan–FLG–COOH, and gelatin–chitosan–FLG–PEG composite films at (a) pH 4.5, (b) pH 7.0, and (c) pH 8.0, mimicking different physiological conditions.

vaginal mucosa, and tumor microenvironment. The significant drug release at pH 7.0, as shown in Fig. 10b, reflects the suitability of the composite films for systemic drug delivery under physiological conditions, including the colon, tissues, and bloodstream.[54,55] Moreover, the most predictable and sustained drug delivery was observed at a pH of 8.0 (Fig. 10c), due to the pH-responsive behavior of chitosan. It becomes less protonated and more compact in alkaline environments, thereby maintaining the structural integrity of the polymeric matrix, indicating its suitability as a drug carrier under alkaline conditions, such as those in the small intestine and chronic wounds.[56,57]

© 2025 The Author(s). Published by the Royal Society of Chemistry

Open Access Article. Published on 24 November 2025. Downloaded on 6/7/2026 10:33:14 AM.
This article is licensed under a Creative Commons Attribution-NonCommercial 3.0 Unported Licence.

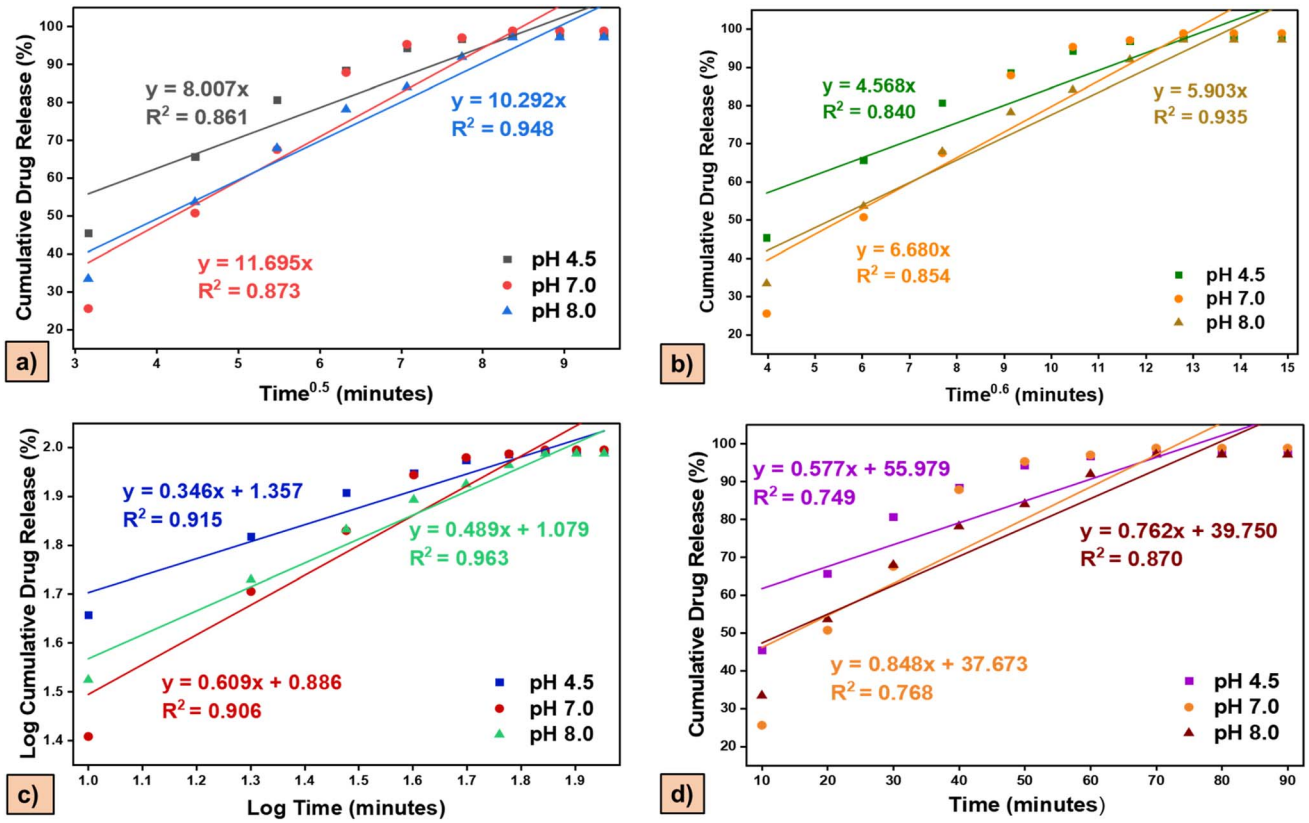

Fig. 11 Graph showing fitted line of the drug release from gelatin–chitosan–FLG–PEG composite using four kinetics models, including (a) Higuchi model, (b) Ritger–Peppas model, (c) Korsmeyer–Peppas model, and (d) zero order model at varying pH conditions.

The gelatin–chitosan–FLG–PEG film demonstrated faster and more complete drug release than both the gelatin–chitosan–FLG–COOH and plain gelatin–chitosan films, with approximately 98% of Uromitexan (Mesna) released within 80 minutes. This enhancement is attributed to the increased hydrophilicity of the composite films resulting from the presence of PEG. Additionally, PEG functionalization offers biological advantages, including reduced opsonization and enhanced biocompatibility and stability under various physiological conditions, making it a promising biomaterial for localized, rapid, and sustained drug delivery applications.[16,19]

3.9. Drug release kinetics

Mathematical modeling of drug release was performed to predict whether the release mechanism is controlled by diffusion, chemical interaction, osmotic pressure, matrix erosion, swelling, or dissolution dynamics, which is essential for designing a drug delivery system (DDS) with optimal therapeutic efficacy.[58,59] The linear fit graphs of the four kinetic models, along with the calculated parameters, are presented in Fig. 11 and summarized in Table 1.

The drug release from the gelatin–chitosan–FLG–PEG composite followed the Korsmeyer–Peppas model, as evidenced by R^2 values ranging from 0.915 to 0.963 across different conditions. In this model, $n \leq 0.5$ corresponds to Fickian diffusion from a non-swellable matrix, $0.5 < n < 1$ corresponds to an anomalous mechanism involving both diffusion and polymer relaxation or erosion, $n = 1$ signifies zero-order release, and $n > 1$ denotes transport involving only erosion mechanisms.[60] In our study, the n-value at pH = 4.5 and pH = 8.0 was found to be 0.346 and 0.489, respectively, indicating Fickian diffusion. However, at pH = 7.0, the n-value increases to 0.609, suggesting the involvement of both diffusion and erosion mechanisms in non-Fickian diffusion. The pH-responsive shift from Fickian to

Table 1 The measured data for the rate constants (K), correlation coefficients (R^2), and diffusional exponent (n; Korsmeyer–Peppas) for four fitted kinetic models

	Higuchi model		Ritger–Peppas model		Korsmeyer–peppas model			Zero-order model	
Samples	K	R^2	K	R^2	n	K	R^2	K	R^2
pH 4.5	8.007	0.861	4.568	0.84	0.346	22.751	0.915	0.577	0.749
pH 7.0	11.695	0.873	6.680	0.854	0.609	7.6913	0.906	0.848	0.768
pH 8.0	10.292	0.948	5.903	0.935	0.489	11.995	0.963	0.762	0.870

© 2025 The Author(s). Published by the Royal Society of Chemistry

Open Access Article. Published on 24 November 2025. Downloaded on 6/7/2026 10:33:14 AM.
This article is licensed under a Creative Commons Attribution-NonCommercial 3.0 Unported Licence.

non-Fickian diffusion is due to pH-dependent swelling and protonation/deprotonation of amine groups.[21,61]

At pH 4.5, the amines of chitosan are fully protonated, generating osmotic pressure and electrostatic repulsion within the matrix, leading to expansion of the polymer network, swelling, and improved chain flexibility.[62–64] At pH = 7.0, the free amino groups are less protonated, which reduces the repulsion between functional groups, leading to less expanded, less swollen chitosan chains, and the chain relaxation rate is reduced compared to that of the lower pH.[65,66] In this case, solvent diffusion and polymer relaxation occur at similar rates, leading to non-Fickian (anomalous) diffusion; hence, drug release depends on both the diffusion and polymer relaxation rates. However, at pH = 8.0, the deprotonation of chitosan amines leads to further reduction in the swelling and lowers the polymer chain relaxation rate, which reverts the release to diffusion-controlled Fickian transport.[21,61]

The Higuchi model ($R^2 = 0.9469$) provided a good fit at pH 8.0, indicating that drug release occurs from a non-swelling polymeric matrix at a constant drug diffusivity, regardless of whether the matrix is solid or semi-solid. Although the Higuchi model exhibited high R^2 values under basic conditions, its assumptions are violated at higher pH because the swelling matrix at acidic conditions changes its diffusivity over time.[20,67–69] The zero-order model showed the lowest linearity across all pH levels and, hence, is not a suitable fit for our study.

In the case of the Korsmeyer–Peppas model, the coefficient of determination (R^2) was found in the decreasing order to be 0.963, 0.915, and 0.906 at pH = 8.0, 4.5, and 7.0, respectively. This indicates that the model is best fitted for basic pH conditions. The drug release rate constant (K) also exhibited a similar trend, with the highest value of 22.751 found at pH 4.5, indicating faster drug release under acidic conditions, likely due to higher protonation and swelling, as stated above. At pH 8.0 and 7.0, the K value decreased to 11.995 and 7.6913, respectively, indicating lower drug diffusion, which is likely due to reduced swelling and increased matrix compactness. These findings support the idea that the drug release mechanism and kinetics are strongly influenced by the pH of the medium.

4. Conclusions

This paper focuses on the synthesis and characterization of functionalized few-layer graphene-incorporated gelatin–chitosan bio-composite films and their subsequent efficiency in drug delivery systems. FTIR spectroscopy confirmed the successful functionalization of FLG, exhibiting distinct peaks for the carboxy (–COOH) ester and polyethylene glycol (PEG), indicating the synthesis of FLG–COOH and FLG–PEG, respectively. In addition, the FTIR spectrum confirmed that the FLG was successfully incorporated into the polymer matrix due to strong intermolecular interactions, such as hydrogen bonding between the functional groups of FLG and the amino/hydroxy/carboxy groups of chitosan and gelatin. FE-SEM analysis confirmed that PEG-functionalized FLG is homogeneously dispersed within the gelatin–chitosan matrix, where the polymer chains wrap around the nanosheets, reduce aggregation, and create a smoother and uniform film. Furthermore, one of the remarkable findings includes enhanced tensile strength, elongation at break, and marked thermal stability, as proven by TGA and DSC analysis. The functionalized composites proved to be highly biocompatible, as indicated by the relatively low cytotoxicity measure in HeLa cells, which resulted in 95% HeLa cell viability of the secondary functionalized FLG. Antimicrobial susceptibility tests demonstrated clear inhibition zones for both Gram-positive and Gram-negative bacteria, indicating very high antimicrobial activity of the resultant composites. The drug release reports showed that the functionalization of FLG significantly accelerated drug release. The FLG–PEG composite exhibited complete drug release at pH levels of 4.5, 7.0, and 8.0, mimicking different physiological conditions. Kinetic modeling demonstrated that the Korsmeyer–Peppas equation best characterizes the release process, exhibiting a transition between Fickian and non-Fickian release behaviors as the pH of the release medium changes. In general, the effective functionalization of FLG and subsequent incorporation into a gelatin–chitosan matrix resulted in a multifunctional, cytocompatible, mechanically robust, pH-responsive drug delivery system with high potential for future biomedical applications.

Ethical statement

The cytotoxic study was conducted in strict accordance with the Guidelines for the Care and Use of Laboratory Animals of the Centre for Advanced Research in Sciences (CARS) at the University of Dhaka, utilizing their commercial services. The experimental procedures were approved by the Committee on the Ethics of Animal Experiments of the Centre for Advanced Research in Sciences at the University of Dhaka. HeLa cells (a human cervical carcinoma cell line) were used in the cytotoxicity analysis, which was obtained from the CARS.

Author contributions

N. S. conducted experiments, contributed to writing the initial manuscript draft, and interpreted the data. M. H. contributed to manuscript writing, experiments, and reviewing, as well as data visualization and interpretation. M. S. A. wrote the manuscript and performed experiments, data visualization and data interpretation. F. T. contributed to writing and data interpretation. N. K. reviewed the manuscript and provided overall guidance during its preparation. K. S. S. and A. F. M. M. R. designed the study, reviewed the manuscript, and provided overall supervision for the research.

Conflicts of interest

There are no conflicts to declare.

Data availability

The data supporting the findings of this study are available from the corresponding author upon reasonable request.

Open Access Article. Published on 24 November 2025. Downloaded on 6/7/2026 10:33:14 AM. This article is licensed under a Creative Commons Attribution-NonCommercial 3.0 Unported Licence.

Supplementary Information: the SI file includes SEM images of different magnifications and images from disk diffusion assays demonstrating antimicrobial activity. See DOI: https://doi.org/10.1039/d5ra05507e.

Acknowledgements

We acknowledge the partial financial support from the University Grants Commission of Bangladesh (Ref. No. Chemical Science Sub-branch/2022-23/7) under UGC Research Grant 2022–23. We also sincerely thank the Drug Lab of the Centre for Advanced Research in Sciences (CARS), University of Dhaka, for providing laboratory facilities to conduct this research.

References

1 M. Sang, J. Shin, K. Kim and K. J. Yu, Electronic and Thermal Properties of Graphene and Recent Advances in Graphene Based Electronics Applications, *Nanomaterials*, 2019, **9**, 374.
2 D. E. Sheehy and J. Schmalian, Optical transparency of graphene as determined by the fine-structure constant, *Phys. Rev. B:Condens. Matter Mater. Phys.*, 2009, **80**, 193411.
3 Z. Najafi rad, F. Farzad and L. Razavi, Surface functionalization of graphene nanosheet with poly (l-histidine) and its application in drug delivery: covalent vs. non-covalent approaches, *Sci. Rep.*, 2022, **12**, 19046.
4 J. Park, X. Yang, D. Wickramasinghe, M. Sundhoro, N. Orbey, K.-F. Chow and M. Yan, Functionalization of pristine graphene for the synthesis of covalent graphene–polyaniline nanocomposite, DOI:DOI: 10.1039/D0RA03579C.
5 Ş. Taşdemir, Z. G. Morçimen, A. A. Doğan, C. Görgün and A. Şendemir, Surface Area of Graphene Governs Its Neurotoxicity, *ACS Biomater. Sci. Eng.*, 2023, **9**, 3297–3305.
6 M. Hasan, D. Mozumder, S. U. Sams, J. Palit, K. Md. Y. Arafat, Md. S. Quddus, M. Mahmud, L. Pal, L. A. Lucia and K. S. Salem, Ultralow-Density Mesoporous PDMS-Doped Graphene Oxide Foam for Cyclic Oil Absorption and FOG Deposition Mitigation, *ACS Appl. Eng. Mater.*, 2025, **3**(4), 998–1011.
7 A. Voznyakovskii, A. Vozniakovskii and S. Kidalov, New Way of Synthesis of Few-Layer Graphene Nanosheets by the Self Propagating High-Temperature Synthesis Method from Biopolymers, *Nanomaterials*, 2022, **12**, 657.
8 L. Zhou, L. Fox, M. Włodek, L. Islas, A. Slastanova, E. Robles, O. Bikondoa, R. Harniman, N. Fox, M. Cattelan and W. H. Briscoe, Surface structure of few layer graphene, *Carbon*, 2018, **136**, 255–261.
9 F. Liu, P. Li, H. An, P. Peng, B. McLean and F. Ding, Achievements and Challenges of Graphene Chemical Vapor Deposition Growth, *Adv. Funct. Mater.*, 2022, **32**(42), 2203191.
10 C. Liao, Y. Li and S. C. Tjong, Graphene Nanomaterials: Synthesis, Biocompatibility, and Cytotoxicity, *Int. J. Mol. Sci.*, 2018, **19**, 3564.
11 S. Qamar, N. Ramzan and W. Aleem, Graphene dispersion, functionalization techniques and applications: A review, *Synth. Met.*, 2024, **307**, 117697.
12 T. A. Seidu, P. T. Kutoka, D. O. Asante, M. A. Farooq, R. N. Alolga and W. Bo, Functionalization of Nanoparticulate Drug Delivery Systems and Its Influence in Cancer Therapy, *Pharmaceutics*, 2022, **14**, 1113.
13 M. Kazempour, H. Namazi, A. Akbarzadeh and R. Kabiri, Synthesis and characterization of PEG-functionalized graphene oxide as an effective pH-sensitive drug carrier, *Artif. Cells, Nanomed., Biotechnol.*, 2019, **47**, 90–94.
14 L. Ou, B. Song, H. Liang, J. Liu, X. Feng, B. Deng, T. Sun and L. Shao, Toxicity of graphene-family nanoparticles: a general review of the origins and mechanisms, *Part. Fibre Toxicol.*, 2016, **13**(1), 57.
15 S. Sharmeen, A. M. Rahman, M. M. Lubna, K. S. Salem, R. Islam and M. A. Khan, Polyethylene glycol functionalized carbon nanotubes/gelatin-chitosan nanocomposite: An approach for significant drug release, *Bioact. Mater.*, 2018, **3**, 236–244.
16 J. Krishnan, P. Poomalai, A. Ravichandran, A. Reddy and R. Sureshkumar, A Concise Review on Effect of PEGylation on the Properties of Lipid-Based Nanoparticles, *Assay Drug Dev. Technol.*, 2024, **22**, 246–264.
17 S. Y. Fam, C. F. Chee, C. Y. Yong, K. L. Ho, A. R. Mariatulqabtiah and W. S. Tan, Stealth coating of nanoparticles in drug-delivery systems, *Nanomaterials*, 2020, **10**, 787.
18 O. Catanzano, G. Gomez d'Ayala, A. D'Agostino, F. Di Lorenzo, C. Schiraldi, M. Malinconico, R. Lanzetta, F. Bonina and P. Laurienzo, PEG-crosslinked-chitosan hydrogel films for *in situ* delivery of *Opuntia ficus-indica* extract, *Carbohydr. Polym.*, 2021, **264**, 117987.
19 M. Kazempour, H. Namazi, A. Akbarzadeh and R. Kabiri, Synthesis and characterization of PEG-functionalized graphene oxide as an effective pH-sensitive drug carrier, *Artif. Cells, Nanomed., Biotechnol.*, 2019, **47**, 90–94.
20 M. Mahmud, A. F. M. M. Rahman, K. S. Salem, Md. L. Bari and H. Qiu, Architecting Ultrathin Graphitic C_3 N_4 Nanosheets Incorporated PVA/Gelatin Bionanocomposite for Potential Biomedical Application: Effect on Drug Delivery, Release Kinetics, and Antibacterial Activity, *ACS Appl. Bio Mater.*, 2022, **5**, 5126–5139.
21 F. E. Koc and T. G. Altıncekic, Investigation of gelatin/chitosan as potential biodegradable polymer films on swelling behavior and methylene blue release kinetics, *Polym. Bull.*, 2021, **78**, 3383–3398.
22 C. Qiao, X. Ma, J. Zhang and J. Yao, Molecular interactions in gelatin/chitosan composite films, *Food Chem.*, 2017, **235**, 45–50.
23 K. Aleksandr, L. Mikhail and P. Aleksandr, Self-Assembled Hydrogel Based on (Bio)polyelectrolyte Complex of Chitosan–Gelatin: Effect of Composition on Physicochemical Properties, *Gels*, 2024, **10**, 786.
24 W. Thakhiew, M. Champahom, S. Devahastin and S. Soponronnarit, Improvement of mechanical properties of chitosan-based films via physical treatment of film-forming solution, *J. Food Eng.*, 2015, **158**, 66–72.
25 M. U. A. Khan, Z. Yaqoob, M. N. M. Ansari, S. I. A. Razak, M. A. Raza, A. Sajjad, S. Haider and F. M. Busra, Chitosan/

© 2025 The Author(s). Published by the Royal Society of Chemistry

Open Access Article. Published on 24 November 2025. Downloaded on 6/7/2026 10:33:14 AM. This article is licensed under a Creative Commons Attribution-NonCommercial 3.0 Unported Licence.

Poly Vinyl Alcohol/Graphene Oxide Based pH-Responsive Composite Hydrogel Films: Drug Release, Anti-Microbial and Cell Viability Studies, *Polymers*, 2021, **13**, 3124.

26 N. S. H. Dao, V. H. Nguyen, D. T. Do and D. L. Nguyen, Scale-up synthesis of mesna using alkyl trithiocarbonate approach, *Pharm. Sci. Asia*, 2018, **45**, 55–65.

27 G. Liu, H. Qin, T. Amano, T. Murakami and N. Komatsu, Direct Fabrication of the Graphene-Based Composite for Cancer Phototherapy through Graphite Exfoliation with a Photosensitizer, *ACS Appl. Mater. Interfaces*, 2015, **7**, 23402–23406.

28 K. Salem, M. Lubna, A. F. M. M. Rahman, M. NurNabi, M. R. Islam and M. Khan, The effect of multiwall carbon nanotube additions on the thermo-mechanical, electrical, and morphological properties of gelatin–polyvinyl alcohol blend nanocomposite, *J. Compos. Mater.*, 2014, **49**, 1379–1391.

29 T. Islam, K. S. Salem, S. Biswas, P. Haque, S. H. Rimu and M. M. Rahman, Preparation of Carbon Nanotube Reinforced Gelatin-Chitosan-Hydroxyapatite Biocomposite for Bone Tissue Engineering, *Op Acc J Bio Eng & Bio Sci*, 2018, **1**(3), 113.

30 J. Hudzicki, Kirby-Bauer disk diffusion susceptibility test protocol, *Am. Soc. Microbiol.*, 2009, **15**, 1–23.

31 R. Kumari and M. Nath, Synthesis, characterization and binding studies of novel diorganotin(IV) complexes of sodium 2-mercaptoethanesulfonate: KUMARI & NATH; Diorganotin(IV) Complexes of MESNA, *Appl. Organomet. Chem.*, 2018, **32**, e4365.

32 B. C. Smith, *Fundamentals of Fourier Transform Infrared Spectroscopy*, CRC Press, 2011.

33 M. A. Al Islam, A. Rahman, S. Iftekhar, K. S. Salem, N. Sultana and M. L. Bari, Morphology, thermal stability, electrical, and mechanical properties of graphene incorporated poly (vinyl alcohol)-gelatin nanocomposites, *Int. J. Compos. Mater.*, 2016, **6**, 172–182.

34 D. Hazarika, K. Gupta, M. Mandal and N. Karak, High-Performing Biodegradable Waterborne Polyester/Functionalized Graphene Oxide Nanocomposites as an Eco-Friendly Material, *ACS Omega*, 2018, **3**, 2292–2303.

35 V. Chabot, B. Kim, B. Sloper, C. Tzoganakis and A. Yu, High yield production and purification of few layer graphene by Gum Arabic assisted physical sonication, *Sci. Rep.*, 2013, **3**, 1378.

36 J. Cho, M.-C. Heuzey, A. Bégin and P. J. Carreau, Viscoelastic properties of chitosan solutions: Effect of concentration and ionic strength, *J. Food Eng.*, 2006, **74**, 500–515.

37 J. Xu, K. Liu, W. Chang, B.-S. Chiou, M. Chen and F. Liu, Regulating the Physicochemical Properties of Chitosan Films through Concentration and Neutralization, *Foods*, 2022, **11**, 1657.

38 B. Shi, Z. Hao, Y. Du, M. Jia and S. Xie, Mechanical and barrier properties of chitosan-based composite film as food packaging: A review, *BioResources*, 2024, **19**, 4001–4014.

39 E. Vafaei, M. Hasani, N. Salehi, F. Sabbagh and S. Hasani, Enhancement of Biopolymer Film Properties Using Spermidine, Zinc Oxide, and Graphene Oxide Nanoparticles: A Study of Physical, Thermal, and Mechanical Characteristics, *Materials*, 2025, **18**, 225.

40 B. Shi, Z. Hao, Y. Du, M. Jia and S. Xie, Mechanical and barrier properties of chitosan-based composite film as food packaging: A review, *BioResources*, 2024, **19**, 4001–4014.

41 P. Zhu, Y. Yan, Y. Zhou, Z. Qi, Y. Li and C.-M. Chen, Thermal Properties of Graphene and Graphene-Based Nanocomposites: A Review, *ACS Appl. Nano Mater.*, 2024, **7**, 8445–8463.

42 S. J. Lee, S. J. Yoon and I.-Y. Jeon, Graphene/Polymer Nanocomposites: Preparation, Mechanical Properties, and Application, *Polymers*, 2022, **14**, 4733.

43 S. Suryani, A. Y. Chaerunisaa, I. M. Joni, R. Ruslin, L. O. A. N. Ramadhan, Y. W. Wardhana and S. H. Sabarwati, Production of Low Molecular Weight Chitosan Using a Combination of Weak Acid and Ultrasonication Methods, *Polymers*, 2022, **14**, 3417.

44 K.-H. Liao, S. Aoyama, A. A. Abdala and C. Macosko, Does Graphene Change Tg of Nanocomposites?, *Macromolecules*, 2014, **47**, 8311–8319.

45 S. Eltahir, R. Al Homsi, J. Jagal, I. S. Ahmed and M. Haider, Graphene Oxide/Chitosan Injectable Composite Hydrogel for Controlled Release of Doxorubicin: An Approach for Enhanced Intratumoral Delivery, *Nanomaterials*, 2022, **12**, 4261.

46 R. Zhou and H. Gao, Cytotoxicity of graphene: recent advances and future perspective, *Wiley Interdiscip. Rev. Nanomed. Nanobiotechnol.*, 2014, **6**, 452–474.

47 G. Perini, V. Palmieri, G. Friggeri, A. Augello, M. De Spirito and M. Papi, Carboxylated graphene quantum dots-mediated photothermal therapy enhances drug-membrane permeability, ROS production, and the immune system recruitment on 3D glioblastoma models, *Cancer Nanotechnol.*, 2023, **14**, 13.

48 T. Lammel, P. Boisseaux, M.-L. Fernández-Cruz and J. M. Navas, Internalization and cytotoxicity of graphene oxide and carboxyl graphene nanoplatelets in the human hepatocellular carcinoma cell line Hep G2, *Part. Fibre Toxicol.*, 2013, **10**, 27.

49 H. Sun, C. Jiang, L. Wu, X. Bai and S. Zhai, Cytotoxicity-Related Bioeffects Induced by Nanoparticles: The Role of Surface Chemistry, *Front. Bioeng. Biotechnol.*, 2019, **7**, 414.

50 J. Li, Y. Liu and X. Zhao, Latest research progress on antibacterial properties of chitosan-based nanofibers, *Chem. Eng. J.*, 2025, **517**, 163776.

51 K. Shankar, S. Agarwal, S. Mishra, P. Bhatnagar, S. Siddiqui and I. Abrar, A review on antimicrobial mechanism and applications of graphene-based materials, *Biomater. Adv.*, 2023, **150**, 213440.

52 S. Gurunathan, M. Arsalan Iqbal, M. Qasim, C. H. Park, H. Yoo, J. H. Hwang, S. J. Uhm, H. Song, C. Park, J. T. Do, Y. Choi, J.-H. Kim and K. Hong, Evaluation of Graphene Oxide Induced Cellular Toxicity and Transcriptome Analysis in Human Embryonic Kidney Cells, *Nanomaterials*, 2019, **9**, 969.

53 H.-S. Hsieh, R. Wu and C. T. Jafvert, Light-Independent Reactive Oxygen Species (ROS) Formation through Electron

Open Access Article. Published on 24 November 2025. Downloaded on 6/7/2026 10:33:14 AM. This article is licensed under a Creative Commons Attribution-NonCommercial 3.0 Unported Licence.

Transfer from Carboxylated Single-Walled Carbon Nanotubes in Water, *Environ. Sci. Technol.*, 2014, **48**, 11330–11336.

54 H. Shoukat, K. Buksh, S. Noreen, F. Pervaiz and I. Maqbool, Hydrogels as Potential Drug-Delivery Systems: Network Design and Applications, *Ther. Deliv.*, 2021, **12**(5), 375–396.

55 M. Rajabzadeh-Khosroshahi, M. Pourmadadi, F. Yazdian, H. Rashedi, M. Navaei-Nigjeh and B. Rasekh, Chitosan/agarose/graphitic carbon nitride nanocomposite as an efficient pH-sensitive drug delivery system for anticancer curcumin releasing, *J. Drug Deliv. Sci. Technol.*, 2022, **74**, 103443.

56 F. Pan, G. Giovannini, S. Zhang, S. Altenried, F. Zuber, Q. Chen, L. F. Boesel and Q. Ren, pH-responsive silica nanoparticles for the treatment of skin wound infections, *Acta Biomater.*, 2022, **145**, 172–184.

57 J.-H. Kang, J.-Y. Hwang, J.-W. Seo, H.-S. Kim and U. S. Shin, Small intestine- and colon-specific smart oral drug delivery system with controlled release characteristic, *Mater. Sci. Eng. C*, 2018, **91**, 247–254.

58 N. Kamaly, B. Yameen, J. Wu and O. C. Farokhzad, Degradable Controlled-Release Polymers and Polymeric Nanoparticles: Mechanisms of Controlling Drug Release, *Chem. Rev.*, 2016, **116**, 2602–2663.

59 K. Taylor, T. A. Tabish and R. J. Narayan, Drug Release Kinetics of DOX-Loaded Graphene-Based Nanocarriers for Ovarian and Breast Cancer Therapeutics, *Appl. Sci.*, 2021, **11**, 11151.

60 M. P. Paarakh, P. A. Jose, C. Setty and G. V. Peter, RELEASE KINETICS – CONCEPTS AND APPLICATIONS, *IJPRT*, 2023, **8**(1), 12–20.

61 J. Ostrowska-Czubenko, M. Gierszewska and M. Pieróg, pH-responsive hydrogel membranes based on modified chitosan: water transport and kinetics of swelling, *J. Polym. Res.*, 2015, **22**, 153.

62 J. Cho, M.-C. Heuzey, A. Bégin and P. J. Carreau, Viscoelastic properties of chitosan solutions: Effect of concentration and ionic strength, *J. Food Eng.*, 2006, **74**, 500–515.

63 G. Sun, X.-Z. Zhang and C.-C. Chu, Formulation and characterization of chitosan-based hydrogel films having both temperature and pH sensitivity, *J. Mater. Sci. Mater. Med.*, 2007, **18**, 1563–1577.

64 J. Guzmán, I. Saucedo, R. Navarro, J. Revilla and E. Guibal, Vanadium Interactions with Chitosan: Influence of Polymer Protonation and Metal Speciation, *Langmuir*, 2002, **18**, 1567–1573.

65 H. S. Kaçoğlu, Ö. Ceylan and M. Çelebi, Determination of Swelling Kinetics and Diffusion Mechanisms of Chemically Crosslinked Porous Chitosan Hydrogels, *Open J. Nano*, 2024, **9**, 106–118.

66 M. Gierszewska-Drużyńska, Mechanism of water diffusion into noncrosslinked and ionically crosslinked chitosan membranes.

67 A. Mráček, The Measurement of Polymer Swelling Processes by an Interferometric Method and Evaluation of Diffusion Coefficients, *Int. J. Mol. Sci.*, 2010, **11**, 532–543.

68 H. Baishya, R. Gouda and Z. Qing, Application of Mathematical Models in Drug Release Kinetics of Carbidopa and Levodopa ER Tablets, *J. Dev. Drugs*, 2017, **6**(2), 1–8.

69 G.-H. Son, B.-J. Lee and C.-W. Cho, Mechanisms of drug release from advanced drug formulations such as polymeric-based drug-delivery systems and lipid nanoparticles, *J. Pharm. Investig.*, 2017, **47**, 287–296.

© 2025 The Author(s). Published by the Royal Society of Chemistry